

A New Tip Correction Based on the Decambering Approach

Jens N. Sørensen, Kaya O. Dag and Néstor Ramos-García
DTU Wind Energy, Technical University of Denmark,
2800 Kongens Lyngby, Denmark

Email: jnso@dtu.dk

Abstract: A limitation of the standard Blade Element Momentum (BEM) technique is that it represents the surface loading by an averaged value determined by locally computed airfoil characteristics. Thus, it does not take into account the chord wise distribution of the induction. Likewise, lifting line methods suffer from the problem that the induction from the free wake vortices is only evaluated along a line representing the center of pressure. Hence, the effect from the chord wise distribution of the induction is neglected. As a consequence, the loading in the proximity of the tip is generally found to be overestimated. To remedy this problem, a correction has been developed, which modifies the circulation by taking into account the additional influence of the induction of the free wake vortices. This is done by correcting the circulation, using the so-called decambering effect and thin-airfoil theory. The correction is implemented as an additional correction to the Prandtl tip correction. Where the Prandtl tip correction serves to correct the axisymmetric momentum theory for a finite number of blades (see Goldstein, 1929), the new model further corrects the blade element model to represent the line distribution by a surface loading. Comparing computations of the new model with results from a ‘standard’ BEM model and computations using a 3D panel code, show that the inclusion of the correction greatly improves the results. The new model also explains some of the discrepancies that earlier on have been observed when using a BEM technique based alone upon standard tip corrections (Shen et al., 2005).

1. Introduction

In a short report published in conjunction with a plenary meeting within a European project, Montgomery (1995) demonstrated that an error is introduced when using lifting line or BEM methods in their usual form. This error is caused by the fact that these methods rely on the blade being represented by a line instead of a surface. Indeed, the downwash induced by the free vortex system in the wake causes a curved streamline along the chord line that effectively corresponds to an additional camber of the airfoil. Since the induction generally will be higher at the trailing edge, which is the line from which the trailing vortices are shed into the wake, than at the leading edge, the aerodynamic consequence is that the effect of the induction from the free vortices is felt as a negative cambering of the airfoil. Hence it tends to increase the zero lift angle and by this decrease the loading. The effect is, just as for the usual tip correction, felt everywhere on the blade, but most significantly close to the tip. In Fig. 1 it is seen how the downwash from the free vortices induce a local velocity field that changes along the chord line. In a lifting line technique, only the velocity component at the center of pressure, which typically is assumed to be the $c/4$ -point, is used to compute the relative velocity and angle of attack. However, as can be seen from the figure there is an additional velocity component, $\Delta w_i = w_i - w_{i,c/4}$, that is negative from the leading edge to the $c/4$ -line and positive from the $c/4$ -line to the trailing edge.



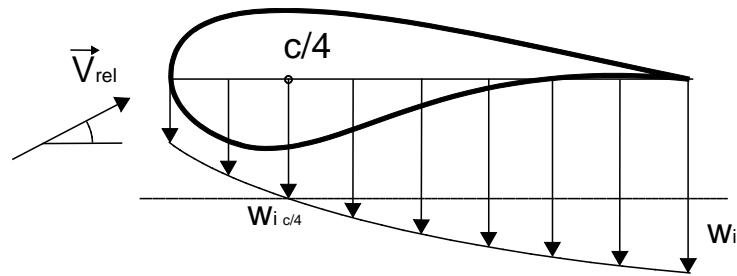


Fig. 1. Downwash due to the induction of the free vortices in the wake

Thus, as seen from the airfoil, the additional velocity is felt as curved streamlines, which consequently represents a negative bending of the airfoil. This is shown in Figs. 2a and 2b, which illustrates how the induced velocity of the free vortex wake is felt as a negative bending of the chord line. This effect was discussed by Montgomery (1995) and referred to as decambering. It should be noted, however, that the term decambering also is employed for the inclusion of post-stall predictions in lifting line or vortex-lattice models (see Mukherjee and Gopalarathnam, 2003).

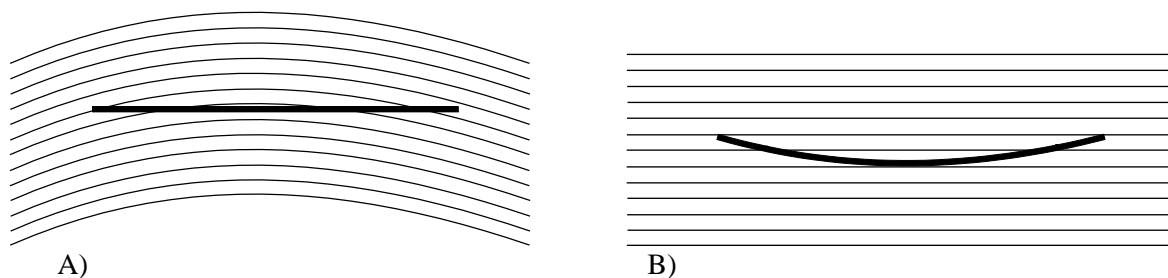


Fig. 2. A) Curved stream lines representing the additional downwash from the induction of the free vortices in the wake; B) The effect from the additional downwash seen as an effective negative bending of the chord line of the airfoil.

In this paper we introduce a technique based on the Biot-Savart induction law, which can be used to determine the effect of decambering. Furthermore, using thin airfoil theory, we develop a simple correction technique by which the loading from lifting line or BEM models can take into account the decambering effect in a similar way as the usual tip correction. By comparing the results from the model with a more advanced numerical technique representing the surface of the rotor, it will be shown that the introduction of a decamber correction in many cases explains most of the discrepancies attained when using the lifting line technique or a BEM model with only a Prandtl tip correction.

2. The decamber correction

As a tool to correct the circulation for the decambering effect we employ thin-airfoil theory. This theory, which is based on a linearization of the potential flow around an airfoil, only serves as an approximate correction to the actual flow. However, for thin airfoils and at moderate angles of attack it has shown to be an accurate and efficient tool for prediction of airfoil performance (Katz and Plotkin, 1991). A basic technique behind thin-airfoil theory is to divide the chord line into a set of evaluation points following a cosine distribution. In the present work, 11 chordwise points were utilized.

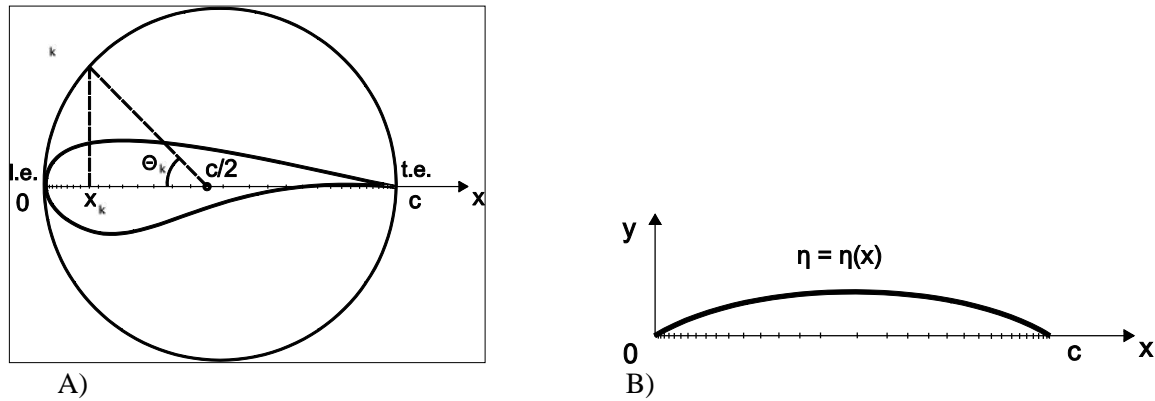


Fig. 3. A) Distribution of evaluation point, x_k , along the chord line; B) Representation of the camber line, $\eta = \eta(x)$.

This distribution is sketched in Fig.3a from which it can be seen that the evaluation point, x_k , is given as

$$x_k = \frac{c}{2}(1 - \cos \theta_k), \quad (1)$$

where

$$\theta_k = \pi \frac{k-1}{M-1}, \quad \text{with } k \in [1, M]. \quad (2)$$

Here M denotes the number of evaluation points. The evaluation points are located along the chord line with the leading edge at $x=0$ ($\theta=0$) and the trailing edge at $x=c$ ($\theta=\pi$). According to thin-airfoil theory the lift coefficient is given as

$$C_l = 2\pi(\alpha - \alpha_{Lo}), \quad (3)$$

where α_{Lo} is the zero-lift angle, which is a function of the camber. According to Katz and Plotkin (1991), from thin-airfoil theory the zero-lift angle can be determined from the following expression,

$$\alpha_{Lo} = -\frac{1}{\pi} \int_0^\pi \frac{d\eta}{dx} c (\cos \theta - 1) d\theta. \quad (4)$$

This expression is usually employed to determine the influence of the camber line on the airfoil characteristics. The camber line of an airfoil is usually a known function, $\eta_c = \eta_c(x)$. However, in the present case the camber line is formed from the additional induction of the free vortices along the chord line. From thin-airfoil theory it is known that the slope of the local (total) velocity is equal to the camber line slope. Hence,

$$\frac{d\eta_c}{dx} = \frac{w}{u}, \quad (5)$$

where (u, w) denotes the velocity components tangential and normal to the chord line, respectively. In order to determine the additional cambering effect from the free vortices in the wake these velocity components are computed from the induction law of Biot-Savart. This is illustrated in Fig. 4, which shows a rotating wing and the associated distribution of circulation due to a simplified vortex system

consisting of trailing vortex lines. Along the 25% chord line of the blade is shown the bound vorticity. The lines extending downwards from the bound vortex line constitute the trailing vortices. The strength of the trailing vortices is determined from the distribution of the circulation of the bound vortex. Representing the bound circulation distribution by discrete values Γ_i , with $i = 1, 2, \dots, N$, with $i = 1$ representing the root and $i = N$ the tip, the associated system of trailing vortices are given as horseshoe vortices. In the case of a rotor blade the trailing vortices are assumed to form a helical spiral with a helical pitch corresponding to the local flow angle. It is the effect from the trailing vortices, which induces a downwash along the chord line of each cross section, that causes the decamber effect. The trailing vortex lines are discretized in a series of linear segments and the induction, i.e. the downwash, is computed along the chord line, which in the span wise direction is located in the midpoint of each horseshoe vortex.

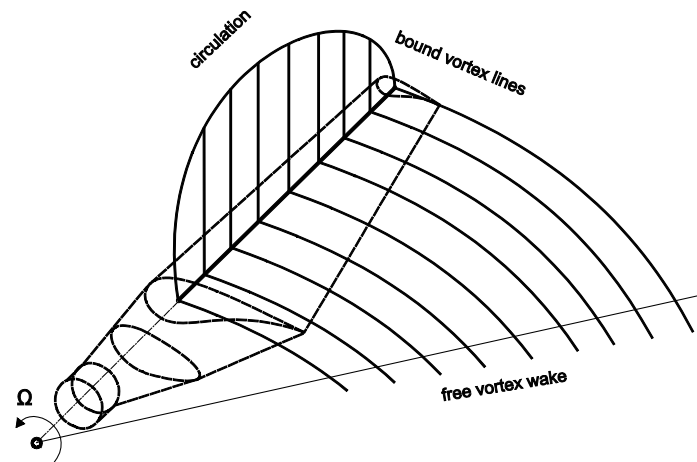


Fig. 4. Rotating wing with associated circulation distribution and vortex lines.

At each evaluation point on the chord line, the induced velocity is determined as the sum of the contribution from the vortex segments starting from the trailing edge of each of the N trailing vortices. Thus, the induced velocity can be written as

$$w_{jk} = \sum_{i=1}^N a_{ijk} \Gamma_i, \quad u_{jk} = \sum_{i=1}^N b_{ijk} \Gamma_i \quad (6)$$

Where a_{ijk} refers to the induced normal velocity on evaluation point k on chord line j due to the induction from vortex i with unit strength, and w_{jk} is the corresponding induced velocity from all the vortices, each of strength Γ_i . Likewise, b_{ijk} refers to the induced velocity in the tangent direction to the chord line. Assuming that the center of pressure is located at the $c/4$ point, the additional camber line slope is determined by subtracting the $c/4$ induction from the local induction. Thus, at each control point the additional slope due to the decamber effect reads

$$\left. \frac{d\eta}{dx} \right|_{jk} = \frac{w_{jk} - w_{j,c/4}}{\|V_{rel,j}\| \cos \alpha_j + u_{jk} - u_{j,c/4}}, \quad (7)$$

where $w_{j,c/4} = \sum_{i=1}^N a_{ij,c/4} \Gamma_i$ and $u_{j,c/4} = \sum_{i=1}^N b_{ij,c/4} \Gamma_i$, with $a_{ij,c/4}$ referring to the induced normal velocity on the c/4-point of chord line j due to the interaction from unit vortex i and $b_{ij,c/4}$ the same for the tangential velocity. Combining eqs. (3) - (7), we get the following formula for correcting the lift coefficient at cross section 'j':

$$\Delta C_{l,j} = 2\Delta\theta \sum_{k=1}^M \frac{(w_{jk} - w_{j,c/4})(\cos\theta_k - 1)}{V_{rel,j} \cos\alpha_j + (u_{jk} - u_{j,c/4})}, \quad (8)$$

where $\Delta\theta = \pi / (M - 1)$. In order to correct directly on the circulation distribution, we employ the Kutta-Joukowski theorem,

$$\Gamma = \frac{1}{2} c V_{rel} C_l. \quad (9)$$

Combining eq. (8) and (9), assuming that $(u_{jk} - u_{j,c/4}) \ll V_{rel,j}$, results in the following correction formula

$$\Delta\Gamma_j = \frac{\Delta\theta \cdot c_j}{\cos\alpha_j} \sum_{k=1}^M (w_{jk} - w_{j,c/4})(\cos\theta_k - 1). \quad (10)$$

Eqs. (6) and (10) forms the final set of equations for correcting the circulation due to the decambering effect of the free wake vortices. It is easily seen that the system constitutes an implicit set of equations, as the induced velocity depends on the circulation being corrected. The system may either be solved iteratively or as a full matrix system.

3. Aerodynamic modelling

In this section we present different aerodynamic wing models to validate the decambering model and to show how the introduced correction for decamber is applied in practice. In particular, we introduce the lifting line method and the Blade-Element Momentum (BEM) technique, which both will be used in connection with the new tip correction. To validate the model we employ a 3D panel method, which will also be introduced.

3.1 Lifting line method

In the lifting line method the vorticity on the wing and wake are represented by horseshoe vortices in a way similar to the sketches shown in Fig. 4. The induction from the trailing vortices is computed from the Biot-Savart law and the local relative velocity is subsequently computed at the c/4-point and employed to compute the local angle of attack. The resulting lift coefficient distribution is then determined from tabulated airfoil data. In order to determine the strength of the trailing vortices we employ the Kutta-Joukowski theorem, eq. (9), which subsequently is corrected for the influence of decamber by the correction term in eq. (10). It is clearly seen that this technique is very well suited to include the influence of decamber as we are employing the same vortex system for computing the angle of attack as for computing the downwash forming the input to the decamber correction. In the present implementation the overall numerical technique for determining the circulation distribution is iterative, and the free vortices in the wake are prescribed to be located in the plane of the wing.

3.2 The Blade-Element Momentum (BEM) method

The BEM method was developed by Glauert (1935) as a practical way to analyse and design rotor blades. In the BEM method the interference factors, a and a' , are introduced as follows

$$a = 1 - u_R / U_0 \text{ and } a' = \frac{u_\theta}{2\Omega r}, \quad (11)$$

where u_R is the axial velocity in the rotor plane, U_0 is the wind speed, u_θ is the rotational velocity in the wake just after the rotor, and Ωr is the local tangential velocity of the rotor at position r . The loading is computed by combining a local blade element consideration using tabulated 2-dimensional airfoil data and the 1-dimensional momentum theorem. Carrying out the analysis (see e.g. Hansen, 2008), the following relations are obtained

$$a = \frac{1}{4F \sin^2 \phi / (\sigma C_l \cos \phi) + 1}, \quad (12)$$

and

$$a' = \frac{1}{4F \sin \phi \cos \phi / (\sigma C_l \sin \phi) - 1}, \quad (13)$$

where the solidity $\sigma = N_b c / 2\pi r$, with N_b denoting the number of blades. $\phi = \phi(r)$ is the local flow angle, $\tan \phi = \frac{U_0(1-a)}{\Omega r(1+a')}$, and F is the Prandtl ‘tip correction’ factor to account for a finite number of blades,

$$F = \frac{2}{\pi} \cos^{-1} \left[\exp\left(-\frac{N_b(R-r)}{2r \sin \phi}\right) \right], \quad (14)$$

where R is the radius of the rotor. Eqs. (12) – (14) are solved iteratively at each cross section, using tabulated airfoil data to determine the local flow properties. After each iteration the decamber correction is introduced by modifying the circulation using eq. (10). The induction coefficients in eq. (6) are determined by computing the induction from the trailing vortices in the wake. These are represented by a number of helical segments, which are released from the trailing edge with the local flow angle, ϕ , and followed a certain distance downstream in the wake.

3.3 The vortex panel method

This method is introduced in order to validate the developed correction. In the panel method the surface of the wing body is simulated by a distribution of quadrilateral singularities satisfying the no-penetration velocity condition. In the present work we employ both the inviscid and the viscous version of the in-house developed MIRAS code (Ramos-Garcia et al., 2013a). In the inviscid part of the model the problem is considered in two regions: the surface, which is represented by quadrilateral sources and dipoles, and the wake, which is modeled by vortex filaments. The vortex wake is released at the trailing edges using the unsteady Kutta-Joukowski condition of zero trailing edge loading. To satisfy this condition, at each time step a quadrilateral panel with a doublet distribution is created as the first wake panel for each one of the span-wise stations. The strength of these panels is equal to the difference between the corresponding upper and lower trailing edge quadrilateral doublets. The filaments are subsequently convected downstream according to the induction law of Biot-Savart, introducing a viscous core model to approximate viscous diffusion and thus including vortex core growth and vortex straining. More details about the model, including a thorough validation, can be found in Ramos-Garcia et al. (2013a, 2013b).

4. Results and Discussion

In this section we validate the new tip correction against results obtained from the MIRAS code. The computations are carried out both for planar wings and rotating wind turbine blades. In the following, for comparison purposes, the circulation is made dimensionless by free-stream velocity and radius.

4.1 Planar translating wing

Here we compare results from the lifting line method described in section 3.1 with the MIRAS panel code. For comparison the computations are carried out both with and without the new tip correction. The example considered is a planar wing with a constant chord consisting of NACA 4412 airfoil sections at various aspect ratios. From inviscid computations using Q³UIC, which can be seen as a 2D version of the MIRAS code, the lift coefficient for 2D airfoil sections is computed as $C_l \cong 2\pi \cdot (1.1\alpha + 0.08)$ for the NACA 4412 airfoil. This is subsequently used for obtaining the initial circulation distribution given by eq. (9). In Fig. 5 we compare computed circulation distributions for the wing at aspect ratios 6 and 10. The pure lifting-line and the decambering correction applied to the lifting-line results are in the figures referred to as 'LLT' and 'decam-LLT', respectively. As the circulation distribution is symmetric, we only depict one half of the distribution. It is clearly seen that the inclusion of the decambering effect makes a big difference. Generally, the lifting line technique is over-predicting the circulation with 10-15%, whereas the inclusion of the decambering correction ensures a circulation distribution that within plotting accuracy corresponds to what is obtained when using a full panel discretization of the surface.

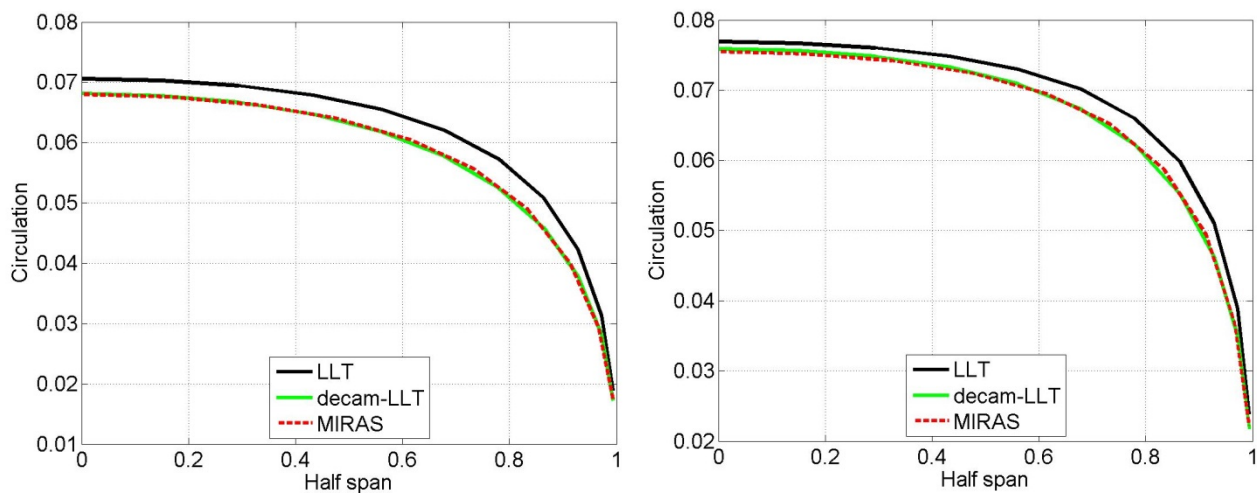


Fig.5. Circulation distributions on planar wings for NACA 4412 airfoils at different aspect ratios. Left: Aspect Ratio = 6; Right: Aspect Ratio = 10.

4.2 Rotating wing: Influence of number of blades

To validate the effect of using the decamber correction on a rotating wing, we employ the correction together with the BEM method. In this method it is still necessary to use the Prandtl tip correction to correct for finite number of blades in the momentum theory. Hence, it is required to apply both the Prandtl tip correction and the decamber correction. In the first part of the study we wish to study the influence of different number of blades. As a consequence, we have designed two simplified wind turbine rotors equipped with two and three blades. The rotor blades were designed using the technique for designing aerodynamically optimum planforms outlined in Burton et al. (2002).

To simplify further the geometry, the blade is everywhere assumed to consist of NACA 4412 airfoils which at optimum conditions operate at a tip speed ratio, $\lambda = 6$, and an angle of attack of 3° , corresponding to $C_l = 0.7$. To simplify further, we replace the chord distribution with a linear expression with the same slope as the one computed at the $y = 80\%$ point. For a 3-bladed rotor this results in a blade with a chord length ranging linearly from $0.156R$ at the root to $0.06R$ at the tip. It should be noted that the twist distribution is invariant to the number of blades.

To use the decambering correction in combination with a BEM technique, a helical wake sheet is generated by using the local axial induction values from the BEM calculation to define the helical pitch. In the present work, three full wake revolutions are used to model the wake. However, as shown in Fig. (6), it is sufficient with a quarter of a revolution to achieve convergence.

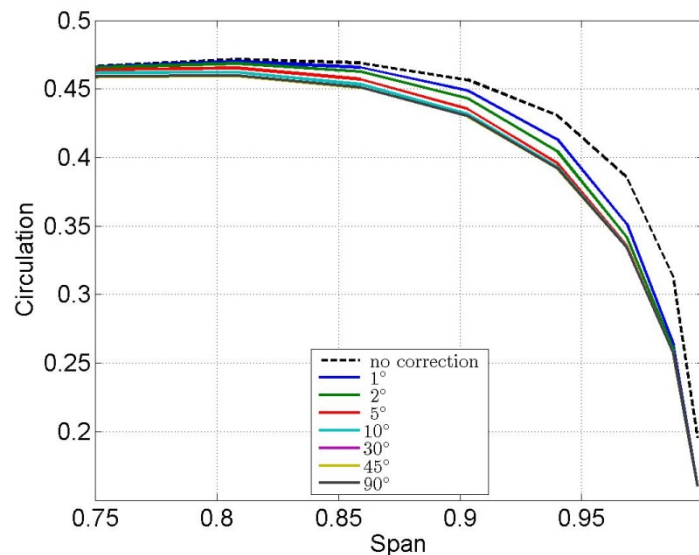


Fig.6. The dependency of the wake length on the decamber correction.

In Fig. (7)-(8) we show computed circulation distributions for a 2- and 3-bladed rotor. The plots compare BEM results with and without the decambering correction with the MIRAS panel code at tip speed ratios 6 and 9. In all the depicted cases it is clear that the decambering correction makes a big difference. In most cases the improvement in the circulation is in the order of 10%. As can also be seen from the figures, the computations without the decambering correction always over-predict the circulation. Hence, the word decambering should be taken literally in the sense that the effective lift distribution, and by this the circulation, is always being reduced when using the correction.

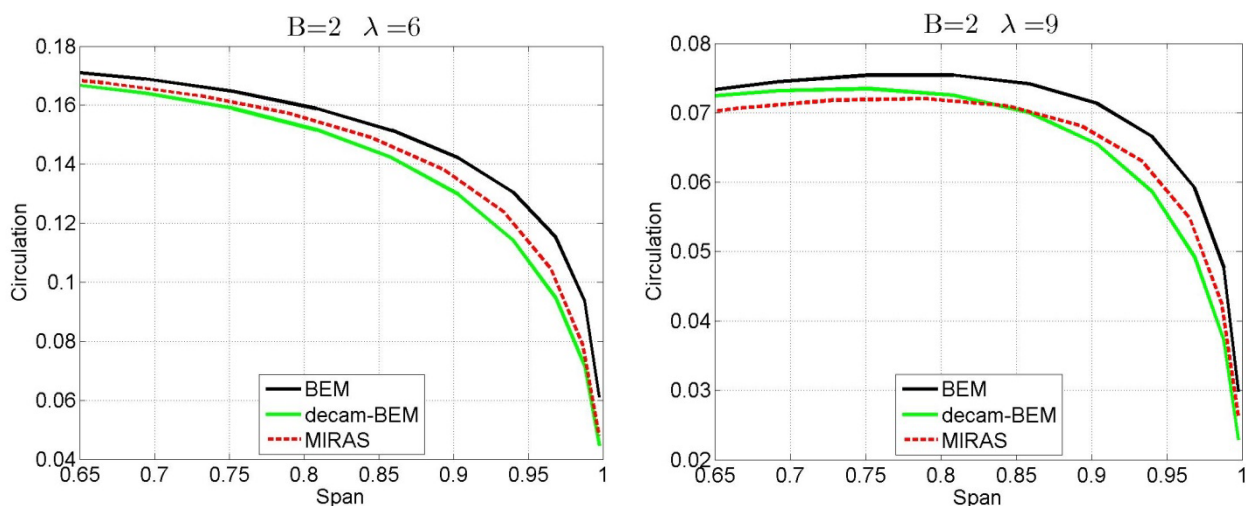


Fig.7. Circulation distributions at the outer part of a 2-bladed rotor; Left: Tip speed ratio = 6; Right: Tip Speed Ratio = 9.

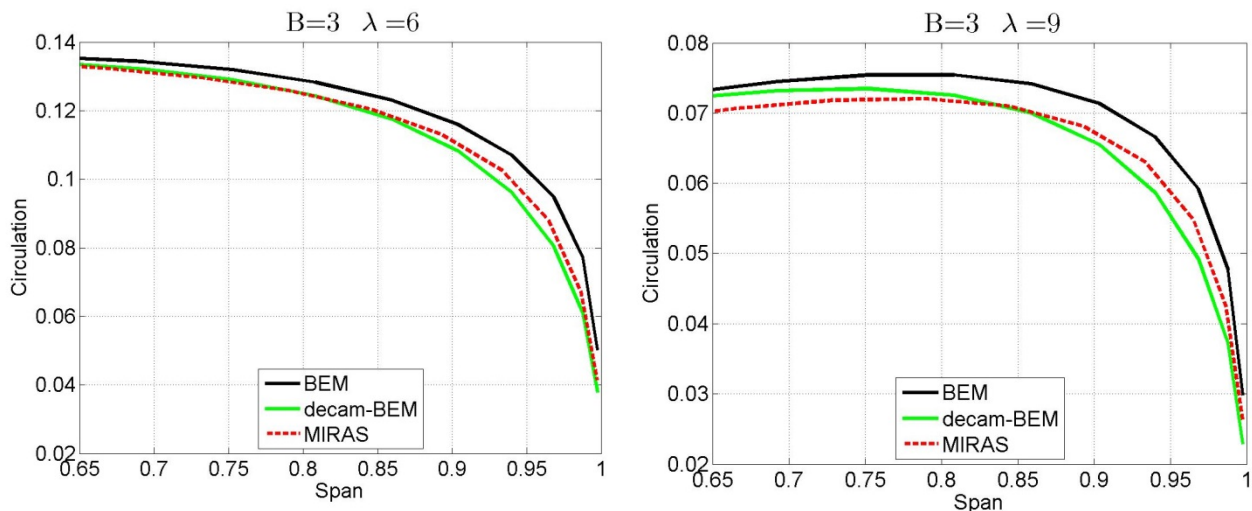


Fig.8. Circulation distributions at the outer part of a 3-bladed rotor; Left: Tip Speed Ratio = 6; Right: Tip Speed Ratio = 9.

4.3 Rotating wing: the NREL 5MW reference case

In order to validate further the decamber correction simulations have been carried out for the NREL 5MW virtual reference rotor. The NREL 5 MW reference wind turbine was designed by Jonkman et al. (2009) in order to have a common test case for comparing different aero-elastic tools. The turbine does not represent an actual wind turbine, but is designed as a good approximation of what an actual wind turbine of the associated size would be like. The diameter of the rotor is 128 m and the blade geometry is based on cylindrical cross sections on the inner part, DU21 - DU40 airfoils at the mid-part and on NACA 64 series airfoils on the outer part. A full description, including airfoil data, can be found in Jonkman et al. (2009).

In the following a comparison between viscous MIRAS simulations, and BEM with and without the decamber correction will be presented for the reference rotor. The viscous MIRAS simulations were performed on a surface mesh consisting of 20 spanwise cells and 160 chordwise cells, and 16 wake revolutions were simulated with an angular discretization of 10° . Viscous effects were taken into account in the potential panel code by employing the transpiration velocity concept and solving the integral boundary layer equations with free laminar to turbulent transition and a turbulent intensity of 0.1%. For more details on the 3D viscous-inviscid coupling technique we refer to Ramos-García et al. (2013a-b). The airfoil polars used in BEM calculations were obtained from 2D viscous-inviscid Q³UIC computations for the local airfoil geometry at the different spanwise locations. More details on the 2D viscous-inviscid interaction technique can be found in Ramos-García et al. (2013c).

In Figure 7 a comparison between the calculated normal and tangential forces for a wind speed of 8 m/s is displayed. The BEM computations, both with and without the refined tip correction, are seen to be in good agreement with the viscous MIRAS computations when comparing the tangential load. It is interesting to note that the additional decamber correction does not have any significant influence on the tangential load, showing that the performance of the rotor is unchanged by the correction. However, comparing the results for the normal load, shows that the decamber correction alleviates the loading by some 7-8% on the outer 10% of the blade. The normal load from the BEM computations, however, seems in all cases to be too high at the outer 30% of the blade, as compared with the MIRAS code. Thus, although the decamber correction improves greatly the prediction of the loading, there is also room for refining the original correction for finite number of blades (the Prandtl correction).

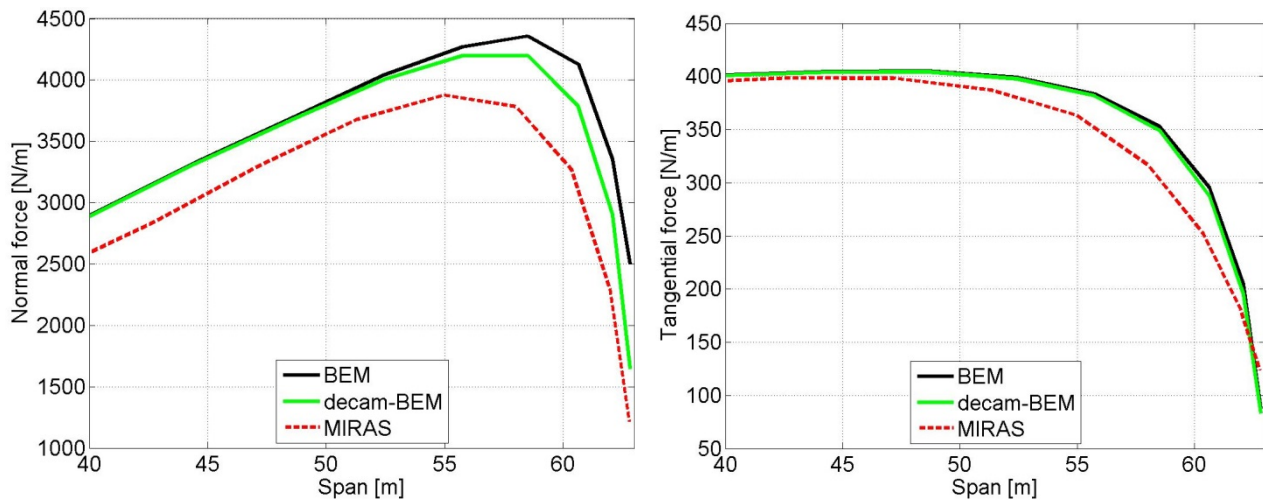


Fig.9. Load distributions on the 5MW NREL reference rotor at 8m/s wind speed. Left: Normal loading; Right: Tangential loading.

Conclusions

A refined tip correction based on thin airfoil theory and the induction from the free vortices in the wake has been developed. The technique corrects the circulation obtained in lifting line or Blade-Element-Momentum (BEM) computations for the difference between a line load and a surface load using the so-called decambering approach. Decambering refers to the fact that the induction from the free vortices in the wake by the airfoil is seen as a negative cambering of the chord line. The resulting correcting formula is derived by combining the Biot-Savart induction law with thin-airfoil theory. The developed correction has been implemented in a lifting line model and in a BEM model, as an additional correction the Prandtl tip correction. Comparisons to results from a 3D panel code show that the new model greatly improves the circulation at the outer part of the rotor blade. The comparison comprises both a planar translating wing as well as 2- and 3-bladed rotors, including the NREL 5MW reference rotor. The correction is most significant for rotors with few blades, corresponding to rotor blades with low aspect ratios. For rotor blades with tapered tip geometries the correction mainly reduces the thrust at the outer part of the blade whereas the change in power performance is insignificant. A main conclusion is that the inclusion of the decamber correction does not change the predicted performance of the rotor, but alleviates the loading by 7-8% at the outer part of the rotor blade.

Acknowledgment

The present work has been carried out with the support of the Danish Council for Strategic Research for the project ‘Center for Computational Wind Turbine Aerodynamics and Atmospheric Turbulence’ (grant 2104-09-067216/DSF) (COMWIND) (<http://www.comwind.org>).

References

- [1] Burton, T., Sharpe, D., Jenkins, N. and Bossanyi, E. (2002) Wind Energy handbook. John Wiley & Sons, Ltd, New York.
- [2] Glauert, H (1935) Airplane propellers, division I. Aerodynamic Theory, 4, pp. 169–360.
- [3] Goldstein, S. (1929) On the vortex theory of screw propellers. Technical report, St. John’s College, Cambridge.
- [4] Jonkman, J., Butterfield, S., Musial, W. and Scott, G. (2009) Definition of a 5-MW Reference Wind Turbine for Offshore System Development. *Technical Report*, NREL/TP-500-38060, National Renewable Energy Laboratory, Golden, Colorado, USA.

- [5] Katz, J., Plotkin, A. (1991) Low-speed aerodynamics. McGraw-Hill, New York.
- [6] Montgomery, B. (1995) De-camber: Explanation of an effect of lift reduction near the tip caused by the local flow around airplane wings or wind turbine tips. Proc. Plenary meeting of the group for Dynamic Stall and 3D Effects a European Union, Joule 2 project. Cranfield Institute of Technology, April 3-4, 1995.
- [7] Mukherjee, R., Gopálathnam, A. (2003) An iterative decambering approach for post-stall prediction of wing characteristics using known section data. AIAA 2003-1097, 41st AIAA Aerospace Sciences Meeting, January 6-9, 2003, Reno.
- [8] Ramos-García, N., Sørensen, J.N. and Shen W.Z. (2013a) "A Strong Viscous-Inviscid Interaction Model for Rotating Airfoils". Published online in J. Wind Energy.
- [9] Ramos-García, N., Sørensen, J.N. and Shen W.Z. (2013b), "Three-Dimensional Viscous-Inviscid Coupling Method for Wind turbine Computations". Published in Wind Energy.
- [10] Ramos-García, N., Sørensen J.N. and Shen W.Z. (2013c) "Validation of a three-dimensional viscous-inviscid interactive solver for wind turbine rotors". Submitted to Renewable Energy: Special Issue in Wind Energy.
- [11] Shen, W.Z., Mikkelsen, R., Sørensen, J.N. and Bak, C. (2005), "Tip loss Corrections for Wind Turbine Computations". Wind Energy, vol. 8, no. 4, pp. 457-475.